HHS Public Access

Author manuscript

J Magn Reson. Author manuscript; available in PMC 2022 June 01.

Published in final edited form as:

J Magn Reson. 2021 June ; 327: 106945. doi:10.1016/j.jmr.2021.106945.

Efficient gradient waveform measurements with variable-prephasing

Kevin D Harkins[a,b,*], **Mark D Does**[a,b]

[a]Biomedical Engineering, Vanderbilt University

[b]Institute of Imaging Science, Vanderbilt University

Abstract

Accurate measurement of gradient waveform errors can often improve image quality in sequences with time varying readout and excitation waveforms. Self-encoding or offset-slice sequences are commonly used to measure gradient waveforms. However, the self-encoding method requires a long scan time, while the offset-slice method is often low precision, requiring the thickness of the excited slice to be small compared to the maximal k-space encoded by the test waveform. This work introduces a hybrid these methods, called variable-prephasing. Using a straightforward algebraic model, we demonstrate that variable-prephasing improves the precision of the waveform measurement by allowing acquisition of larger slice thicknesses. Experiments in a phantom were used to validate the theoretical predictions, showing that the precision of variable-prephasing gradient waveform measurements improves with increasing slice thickness.

1. Introduction

Gradient waveform imperfections—where the actual magnetic gradient field differs from the intended field due to eddy currents, gradient amplifier nonlinearities, or other gradient system errors—are a common source of artifact, particularly for many advanced MRI techniques. Gradient waveform corrections are often necessary to improve image quality in non-Cartesian imaging, including spiral [1, 2], radial [3–6], and radial center-out trajectories [7, 8]. Waveform errors have also been known to cause slice profile distortion for 2D UTE imaging [9–13], and more generally for excitation schemes with a time-varying gradient trajectories [14–17]. For many such acquisitions, image quality depends upon accurate measurement and correction of the gradient field error, and methods to measure gradient waveforms are crucial to improve image quality.

[*]1161 21st Avenue South Medical Center North, AA-1105 Nashville, TN 37232-2310, kevin.harkins@vanderbilt.edu (Kevin D Harkins).

Declaration of interest

The authors have no conflicts of interest in regard to the subject of this manuscript.

Declaration of interests

The authors declare that they have no known competing financial interests or personal relationships that could have appeared to influence the work reported in this paper.

Gradient waveforms can be measured using magnetic field cameras [18, 19], but these systems require specialized hardware and careful calibration. Using standard system hardware, there are two categories of gradient measurement methods. The self-encoding method uses a gradient with known area in between a slice-selective excitation and a test gradient applied during signal reception [20–24]. The test gradient waveform is inferred from the envelope of the signal—e.g., the magnitude of the signal peaks when the time integral of the test gradient cancels that of the self-encoding gradient. The sequence is repeated with different self-encoding gradient amplitudes until the test gradient area be calculated with sufficient temporal resolution. Multi-dimensional variants of this methods have been used for multi-dimensional Because numerous repetitions are required to encode a gradient waveform, the self-encoded method tends to require a long acquisition time.

Alternatively, the offset-slice method estimates the gradient field based upon the signal phase. The change in phase over time is proportional to magnitude of both the applied gradient field and the slice offset from gradient isocenter [25]. If the sequence is repeated with the test gradient on and off, the applied gradient waveform can be distinguished from background sequence contributions and sample-dependent phases. If the sequence is also repeated at multiple slices, both the applied gradient [26] and B_0 eddy currents can be distinguished [27, 28]. While this method is relatively rapid, it also has the lower signal-to-noise ratio (SNR) and requires a thin slice to avoid phase wrapping through the slice.

Here, we introduce a hybrid of the self-encoding and offset-slice method, which we call variable-prephasing. Like the offset-slice method, variable-prephasing uses the change in signal phase from offset slices to calculate the gradient waveform. Similar to the self-encoding method, repeated acquisitions with a variable amplitude self-encoding gradient mitigates the signal loss due to phase wrapping, which, in-turn, allows thicker slices and greater SNR. A algebraic model is presented, which allows the method to be tuned to trade-off scan time for measurement precision. Measurements from a phantom demonstrate improvements to the gradient waveform precision.

2. Theory

The variable-prephasing (VP) pulse sequence is shown in Figure 1, and is comprised of a slice-selective excitation followed by a variable amplitude prephasing gradient, and then an acquisition concurrent with the test gradient waveform. For illustrative purposes, the VP gradient is shown separate from the slice refocusing gradient; however, in practice, the two gradients can be combined to reduce the time between excitation and readout. The slice direction is defined here as the laboratory Z-direction, but could equally be along X- or Y-directions for measurements of X- or Y-direction gradients. A complete measurement from each of N_s slices involves repetition of this sequence with signal with N_v VP gradient amplitudes and N_0 additional reference measurements acquired with both the VP and test gradients turned off.

The acquired signal is

$$S_{n,m}(t) = \int M((z - z_m)/\delta) e^{-i\phi_{n,m}(t,z)} dz \quad (1)$$

where $M(z)$ is the excited slice profile centered at $z = 0$ with unit thickness, z_m is the slice offset of the m-th slice, δ is the slice thickness, and n is the index to the variable pre-phasing step. If the slice profile is conjugate symmetric around z_m, then the phase and magnitude of the signals are separable, resulting in

$$\angle S_{n,m}(t) = \phi_{n,m}(t, z_m), \text{ and} \quad (2)$$

$$|S_{n,m}(t)| = \left| \delta \int M(z) \cos(\delta k_{n,m}(t) z) dz \right|, \quad (3)$$

where

$$k_{n,m}(t) = \frac{\gamma}{2\pi} \int_0^t G_{n,m}(t') dt' \quad (4)$$

The observed signal phase, $\phi_{n,m}(t, z_m)$, contains all contributions from the applied gradient (including induced gradient and B_0 eddy currents) plus static background field shifts.

From the acquisition with the n^{th} VP gradient amplitude from the m^{th} slice, the resonance frequency (in Hz) in the rotating frame can be estimated by 2-point central difference,

$$f_{n,m}(t) = \frac{1}{2\pi} \frac{\phi_{n,m}(t + \Delta t, z_m) - \phi_{n,m}(t - \Delta t, z_m)}{2\Delta t}, \quad (5)$$

where Δt is the receiver sample period. If the effect of the VP gradient on $f(t)$ can be neglected (the consequence of this simplification is outlined in Appendix A), then this frequency can be modeled as depending on the gradient (G) and spatially constant (B) field shifts due to the test gradient, plus a slice-dependent background term, q_m, which originates from background variations in B_0 or residual phases imparted by any other gradients in the sequence.

$$f_{n,m}(t) = \frac{\gamma}{2\pi} [z_m G(t) + B(t)] + q_m(t), \quad (6)$$

where z_m is the slice offset distance of the m-th slice. Defining $f_{0,m}$ as average signal from the N_0 reference acquisitions from the m^{th} slice, we can write Equation 6 for any point in time and all acquisitions as,

$$\mathbf{f} = \mathbf{A}\mathbf{b}$$

$$\begin{bmatrix} f_{1,1} \\ f_{2,1} \\ \vdots \\ f_{N_\mathrm{v},1} \\ f_{1,2} \\ \vdots \\ f_{N_\mathrm{v},2} \\ \vdots \\ f_{N_\mathrm{v},N_\mathrm{S}} \\ f_{0,1} \\ f_{0,2} \\ \vdots \\ f_{0,N_\mathrm{S}} \end{bmatrix} = \begin{bmatrix} z_1 & 1 & 1 & 0 & \cdots & 0 \\ z_1 & 1 & 1 & 0 & \cdots & 0 \\ \vdots & & & & & \\ z_1 & 1 & 1 & 0 & \cdots & 0 \\ z_2 & 1 & 0 & 1 & \cdots & 0 \\ \vdots & & & & & \\ z_2 & 1 & 0 & 1 & \cdots & 0 \\ \vdots & & & & & \\ z_{N_\mathrm{S}} & 1 & 0 & 0 & \cdots & 1 \\ 0 & 0 & 1 & 0 & \cdots & 0 \\ 0 & 0 & 0 & 1 & \cdots & 0 \\ \vdots & & & & \ddots & \\ 0 & 0 & 0 & 0 & \cdots & 1 \end{bmatrix} \begin{bmatrix} G \\ B \\ q_1 \\ q_2 \\ \vdots \\ q_{N_\mathrm{S}} \end{bmatrix}. \tag{7}$$

The rows in Equation 7 iterate first over the N_v VP measurements, and then the N_s slices. The reference measurements are appended as the last N_s rows. The measured phase has a variance that depends on the signal magnitude, $|S_{n,m}|$, which is modulated by the VP gradient,

$$\sigma^2_{\phi_{n,m}} \approx \frac{\sigma^2}{|S_{n,m}|^2}, \tag{8}$$

where σ^2 is the variance of the measured complex signal from a single acquisition [29]. Then the inverse covariance matrix of $\mathbf{f}$, $\mathbf{\Sigma}_\mathbf{f}^{-1}$, is diagonal with the first $N_\mathrm{v}\times N_\mathrm{s}$ elements being proportional to $|S_{n,m}|^2$, and the final N_s elements proportional to $N_0|S_{0,m}|^2$. The maximum likelihood solution to Equation 7 is given by weighted least squares,

$$\hat{\mathbf{b}} = \left(\mathbf{A}^\top \mathbf{\Sigma}_\mathbf{f}^{-1}\mathbf{A}\right)^{-1}\mathbf{A}^\top \mathbf{\Sigma}_\mathbf{f}^{-1}\mathbf{f} \tag{9}$$

(and the proportionality constant in $\mathbf{\Sigma}_\mathbf{f}^{-1}$ cancels). Thus, at any time, t, the measured test gradient waveform amplitude is $\hat{G} = \hat{\mathbf{b}}(1)$, and the variance of $\hat{G}$ normalized to the number of acquisitions is $\sigma^2_{\hat{G}} = \mathbf{\Sigma}_{\hat{\mathbf{b}}}(1,1)$, where

$$\mathbf{\Sigma}_{\hat{\mathbf{b}}} = \frac{1}{N_\mathrm{v} + N_0}\mathbf{A}^\top \mathbf{\Sigma}_\mathbf{f}^{-1}\mathbf{A}^{-1}. \tag{10}$$

Figure 2 compares the theoretical precision of $\hat{G}(1/\sigma_G)$ from offset-slice and VP methods for a rectangular slice profile. Here,

$$|S_n| = \left|\delta \mathrm{sinc}\left(\delta\left(k_\mathrm{G} + k_{\mathrm{v},n}\right)\right)\right|, \tag{11}$$

where sinc(x) = sin(πx)/πx, δ is the slice thickness, and k_G and $k_{v,n}$ are k-space values encoded by the test and VP gradients, respectively. As plotted, precision values are normalized relative to that with $k_G = 0$ and a thin slice, $\delta = 0.25/k_{max}$—this value was chosen because the slice is thin enough relative to the maximum k-space value to provide nearly uniform precision over the entire domain of k_G. The left panel shows the precision for the offset slice method with $k_{max}\delta = 0.25$, 0.5, 1.0, and 2.0. The thin slice shown ($\delta_z = 0.25/k_{max}$) provides low but consistent precision over k-space domain encoded by the test gradient. The thickest slice provides the highest precision near $k_G = 0$, but reduced precision and even zero precision at various points in the k-space domain. The VP method counters the consequences of the thick slice by shifting the signal magnitude, and hence the precision function, across the k-space domain with each VP step. This is illustrated by the dashed line in Figure 2, which shows the precision from the thick slice acquisition shifted when $k_v = -k_{max}/2$. The net precision of the VP method is shown in the right panel of Figure 2 for $N_0 = N_v = 4$ and k_v values uniformly spaced between k_{min} and k_{max}. This plot shows that across the entire k-space domain, precision increases with slice thickness.

Because the precision of the measurement varies across the k-space domain, we define an average measure of the variance over the domain of k_G that can be used to optimize the slice thickness of a given measurement

$$\left\langle \sigma_G^2 \right\rangle \equiv \frac{1}{\Delta k}\int_{k_{min}}^{k_{max}} \sigma_G^2 dk_G . \tag{12}$$

Figure 3 plots $\left\langle \sigma_G^2 \right\rangle$ as a function of slice thickness (δk_{max}) for N_v = 1, 2, 4, and 8 and k_{min} = 0. For each curve, the set of N_v values of k_v are linearly spaced between 0 and $-k_{max}$, and $\left\langle \sigma_G^2 \right\rangle$ normalized relative to lowest $\left\langle \sigma_G^2 \right\rangle$ with $N_v = 1$ (the minimum of the yellow curve, which also represents the minimum noise variance for the offset slice method). In all cases, $\left\langle \sigma_G^2 \right\rangle$ decreases with increasing slice thickness to a point and then phase wrapping causes a loss of signal and $\left\langle \sigma_G^2 \right\rangle$ increases. Increasing N_v allows thicker slices and, in-turn, lower variance of the gradient waveform measurement per excitation.

Figure 4 shows the trade-off of N_0 vs N_v within the fixed total number of acquisitions. For a thin slice ($\delta_z = 0.25/k_{max}$, top set of curves) the variance is optimized at $N_v = N_0$. For a thick slice ($\delta_z = 2/k_{max}$, bottom set of curves), the variance is optimized when N_0 uses approximately 30% of the total scan duration; however, degradation of the variance between N_0 of 30% and 50% of the total scan time is small relative to the improvement in precision provided by the larger slice thickness.

3. Methods

3.1. Test Waveforms to Evaluate Measurement Precision

To compare methods to measure gradient waveforms, test waveforms are needed that highlight regions of noise in the measurement. Precision in gradient waveform measurements is primarily a function of encoded k-space, as illustrated in Figure 2. Chirp or triangular gradient waveforms are often used to characterize gradient system frequency

response because these waveforms can be designed to sample over a range of specific frequencies [30]. Theoretically, precision could be gathered from triangular or chirp waveforms. However, these waveforms are not ideal, as the series of triangles used to evaluate the system response vary in gradient area, and a chirp waveform will traverse the same domain of k-space multiple times. Instead, we used trapezoidal test waveforms to quantitatively compare gradient waveform measurement methods, since these waveforms quickly encode a specific domain in k-space.

3.2. MR Measurements

Gradient waveform measurements were performed on a Bruker 7T scanner, with a 38 mm birdcage coil used for RF excitation and reception. Gradient waveform measurements were performed in a 15 mL tube of distilled water, doped with $CuSO_4$ to a T_1 and $T_2 \approx 300$ ms. Gradient waveform measurements were performed on a trapezoidal test gradient waveform in the Z-direction, with an amplitude of 40mT/m, and duration of 2.35ms, providing $k_{max} \approx 2mm^{-1}$. The readout bandwidth was 250 kHz. A total of seven slices were acquired, at −6, −4, −2, 0, 2, 4, and 6 mm, interspaced within a repetition time of 250 ms. Both offset-slice and VP gradient waveform measurements (with $N_v = N_0 = 4$) had the same scan time, and included $\delta_z = 0.125$, 0.25, 0.5 and 1.0 mm. Gradient waveforms were estimated from the measurements using Equation 9. These measurements were repeated 16 times, and the standard deviation of the waveform measurement ($\hat{\sigma}_G$) was calculated at each point in the waveform.

4. Results

4.1. Variable-prephasing

Figure 5 compares offset-slice based gradient waveform measurements with VP measurements with $N_v = N_0 = 4$, at $k_{max}\delta_z = 0.25$, 0.5, 1.0, and 2.0. For a thin slice ($k_{max}\delta_z = 0.25$), offset-slice and VP measurements provide similar noise variance throughout the entire trapezoidal gradient. As the slice thickness is increased, the offset slice method shows an improvement in the gradient waveform precision at the beginning of the gradient waveform; however, the variance increases significantly as the gradient area increases. In contrast, an increase in slice thickness in the VP measurement shows improved precision of the gradient waveform throughout the entire gradient waveform.

The precision of these measurements ($\left(1/\hat{\sigma}_{G_w}\right)$) is shown in Figure 6, estimated from 16 repetitions of the gradient waveform in Figure 5. The precision was normalized to the thin slice case ($\delta_z = 0.25/k_{max}$) at $k_G = 0$. For the offset slice method, the thin slice provides low but consistent precision over the entire range of k_G/k_{max}. Increasing the slice profile improves the precision at low k_G, but reduces the precision at high k_G. Meanwhile, gradient waveform measurements with VP provides improved precision that is more uniform over the entire range of k_G/k_{max}. These measurements closely match the theoretical predictions shown in Figure 2. A slight decay in the measured precision with increasing k_G is due to T_2^* relaxation, with other differences—particularly in thick slices within the offet-slice method—due to non-rectangular excited slice profile.

5. Discussion

As several advanced MR imaging applications depend upon the fidelity of the gradient system, there is a need for SNR-efficient methods to measure gradient waveforms. The trade-off between maximum gradient area and slice thickness imposed by the offset-slice gradient measurement method limits the utility of the method for measuring gradient waveforms with large gradient areas. For example, using the offset-slice method to measure a readout gradient waveform will require the slice thickness of the gradient waveform measurement to be less than the encoded resolution. For high resolution scans, the thin slice will result in low SNR, requiring many averages and a long scan time to achieve adequate precision. In contrast, the VP method can improve the SNR efficiency of gradient waveform measurements by overcoming the slice thickness limitation of offset-slice method. The method can be applied on any MRI system, and does not require additional hardware.

The variable-prephasing sequence can be considered a generalization of both the self-encoding method and the offset-slice method. If $N_v = 1$, VP is the same as the offset-slice method, capable of providing a fast but low precision estimate of the gradient waveform. For large N_v, the VP sequence is identical to self-encoding, and high precision estimates of the gradient waveforms can be imaged using a Fourier transform [22–24]; although, this method requires a relatively long acquisition time. By using an intermediate value for N_v, the variable-prephasing method can trade off the desired precision of the measurement with total acquisition time.

As part of this work, we demonstrated a weighted least squares framework to estimate the gradient waveform from measurements at multiple slices and multiple VP steps. This framework is useful to optimize the SNR efficiency of these measurements, including the number of measurements with the VP and test gradient off that optimizes the variance of the noise, which was 30 to 50% of the total scan time depending on the slice thickness. While a single channel quadrature coil was used for signal reception in this work, it would be straightforward to extend the model in Equation 7 to optimally estimate gradient waveforms from acquisitions using multi-channel receive coils available on many commercial MRI systems.

Because the VP allows gradient waveform measurements over a larger range in gradient areas, it will enable measurement and correction of gradient waveforms at or near the nonlinear limits of the gradient system. Some previous works have used a linear time-invariant system model of the gradient system (the GIRF) [30–34]. However, the gradient system is only approximately linear over a certain range of gradient amplitude, slew rate, and acceleration rate. As imaging methods use waveforms that approach the nonlinear limits of the gradient system, the fidelity of the GIRF will degrade. Therefore, either such waveforms will need to be individually measured and calibrated, or they will require the development of nonlinear methods to analyze the gradient system.

There is room for further optimization of the VP method. For example, it is possible that precision of the gradient waveform measurement can be further improved by combining measurements acquired at two or more different slice thicknesses. It is also possible that

alternate choices of the N_v VP gradient areas can further improve precision. For some applications, precision may be more important in some regions of k-space than others, which would merit increasing the density of VP measurements in those regions.

While this work neglected higher order terms and cross terms between gradient axes, the VP method can be applied to more general characterization. For example, a recent paper used multi-slice measurements to estimate 2nd & 3rd order spatial gradient terms and used phase encoding in the orthogonal dimensions to estimate cross terms between linear gradients [35]. Variable-prephasing is compatible with this recent method, and could be incorporated to improve precision, particularly in measurement of higher order and cross terms.

While the VP method is able to improve the precision of gradient waveform measurements by increasing the range in useable slice thickness, in some cases larger slices may reduce the accuracy of the method. In particular, the accuracy of this gradient waveform method depends upon conjugate symmetry of the slice profile. Large slices may be less symmetric—either due to partial volume averaging, the presence of background gradients, or air tissue/interfaces—thereby increase bias in the measurements.

Funding

This work was supported by National Institutes of Health grants EB019980 and EB014308.

Appendix A.: Bias of Variable-Prephasing Terms

If the residual contributions from the variable-prephasing gradient lasting into acquisition cannot be neglected, Equation 6 becomes

$$f_{n,m}(t) = \frac{\gamma}{2\pi}\left[z_m G(t) + B(t) + z_m G_{v,n}(t) + B_{v,n}(t)\right] + q_m(t), \quad \text{(A.1)}$$

where $G_{v,n}$ and $B_{v,n}$ are the linear and 0-th order contributions of the n-th VP gradient lasting into the acquired signal. This will result in a biased gradient measurement, but it is straightforward to estimate the magnitude of this bias. In the approximation that the gradient system can be treated as linear time-invariant, a change in the amplitude of the VP gradient (g_n) creates a proportional change $G_{v,n}$ and $B_{v,n}$. Therefore, we can approximate $G_{v,n}(t) \approx c(t)g_n$, and $B_{v,n}(t) \approx d(t)g_n$, where c & d are the magnitude of the residual eddy current. Incorporating this model into the linear system of equations,

$$\mathbf{f} = \mathbf{Ab} + \mathbf{U_v} \quad \text{(A.2)}$$

where

$$\mathbf{U} = \begin{bmatrix} g_1 z_1 & g_1 \\ \vdots & \\ g_{N_\mathrm{V}} z_1 & g_{N_\mathrm{V}} \\ g_1 z_2 & g_1 \\ \vdots & \\ g_{N_\mathrm{V}} z_{N_\mathrm{S}} & g_{N_\mathrm{V}} \\ 0 & 0 \\ \vdots & \\ 0 & 0 \end{bmatrix} \tag{A.3}$$

and

$$\mathbf{v} = \begin{bmatrix} c(t) \\ d(t) \end{bmatrix}. \tag{A.4}$$

The expected bias can be calculated by substituting Equation A.2 into Equation 9

$$\begin{aligned} \left\langle \hat{\mathbf{b}} \right\rangle &= \left(\mathbf{A}^\top \boldsymbol{\Sigma}_\mathbf{f}^{-1} \mathbf{A} \right)^{-1} \mathbf{A}^\top \boldsymbol{\Sigma}_\mathbf{f}^{-1} (\mathbf{A}\mathbf{b} + \mathbf{U}\mathbf{v}) \\ &= \mathbf{b} + \left(\mathbf{A}^\top \boldsymbol{\Sigma}_\mathbf{f}^{-1} \mathbf{A} \right)^{-1} \mathbf{A}^\top \boldsymbol{\Sigma}_\mathbf{f}^{-1} \mathbf{U}\mathbf{v} \end{aligned} \tag{A.5}$$

where the second term is the expected bias of $\hat{\mathbf{b}}$. Therefore, given some estimate of the residual long-lived eddy currents, the expected bias in the estimated gradient waveform can be estimated from the magnitude of the residual eddy current (c).

Such residual long-lived eddy currents are typically low amplitude, can be easily measured using traditional methods (including offset-slice measurements), and are compensated with pre-emphasis. However, this potential bias can also be reduced or effectively eliminated by increasing the delay between the VP gradient and the start of acquisition, potentially at the cost of a small amount of precision due to T_2^* decay. Consider a model of eddy currents as exponential decays. In addition to the magnitude and time constant of the eddy currents, the bias will depend on the duration of VP gradient (τ_v), and the delay between the VP gradient and the start of acquisition (τ_d). Residual eddy currents at the start of acquisition can be estimated as the difference between eddy currents induced from the rising and falling edges of the rectangular VP gradient,

$$c(\tau_\mathrm{d}) = \kappa \left(e^{-\tau_\mathrm{d}/\tau_\mathrm{c}} - e^{-(\tau_\mathrm{d} + \tau_\mathrm{v})/\tau_\mathrm{c}} \right) \tag{A.6}$$

where κ is the magnitude of the eddy current and τ_c is the characteristic time-constant of the eddy current. The fraction of the residual eddy current that lasts into acquisition (c/κ) is plotted in Figure A.7 for $\tau_\mathrm{d}/\tau_\mathrm{c}$ = 0.5, 1.0, 2.0, 4.0 and 8.0. For example, in the case of $\tau_\mathrm{d}/\tau_\mathrm{c}$ = 4.0, the residual eddy current lasting into the acquisition is < 10% of the nominal eddy current amplitude. Equation A.5 provides a straightforward formula to estimate potential measurement bias caused by residual eddy currents from the VP gradient. Using this formula and the gradient waveform measurements presented in this study, Table A.1

compares the average variance of the measured noise with the worst-case bias caused by a 5% amplitude eddy current off a VP gradient with max amplitude 40 mT/m and $\tau_d/\tau_v = 4.0$. For this specific range of cases, the bias is less than the noise in these measurements.

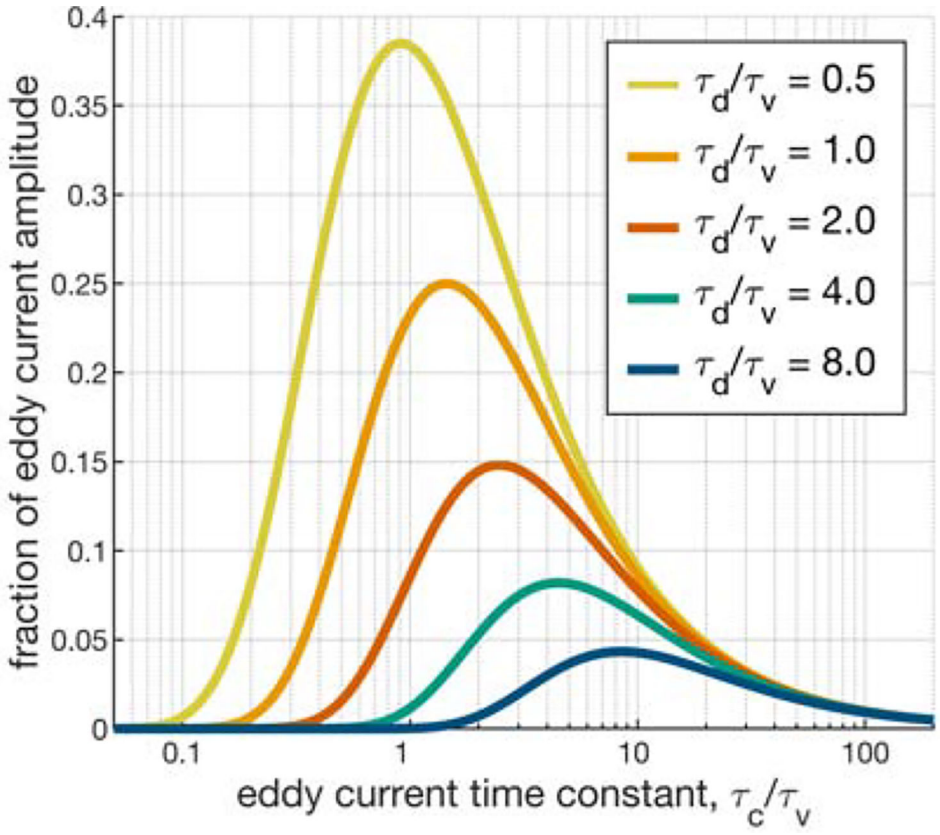

Figure A.7:
If eddy currents off the VP gradient are not negligible, increasing the delay (τ_d) between the VP gradient (with duration τ_v) and the acquisition can be used to reduce the bias of the measured gradient waveform.

Table A.1:

Comparing the standard deviation of the VP gradient waveform measurements with the worst case bias imposed by a 5% eddy current off a 40 mT/m VP gradient with $\tau_d/\tau_v = 4.0$.

δ	$0.25/k_{max}$	$0.25/k_{max}$	$1.0/k_{max}$	$2.0/k_{max}$
$\hat{\sigma}_G$ (mT/m)	2.93	1.74	1.08	0.73
maximum bias (mT/m)	0.11	0.15	0.16	0.16

References

[1]. Tan H, Meyer CH, Estimation of k-space trajectories in spiral MRI, Magnetic Resonance in Medicine 61 (2009) 1396–1404. doi:10.1002/mrm.21813. [PubMed: 19353671]

[2]. Robison RK, Devaraj A, Pipe JG, Fast, simple gradient delay estimation for spiral MRI., Magnetic Resonance in Medicine 63 (2010) 1683–90. doi:10.1002/mrm.22327. [PubMed: 20512872]

[3]. Moussavi A, Untenberger M, Uecker M, Frahm J, Correction of gradient-induced phase errors in radial MRI, Magnetic Resonance in Medicine 71 (2014) 308–312. doi:10.1002/mrm.24643. [PubMed: 23440722]

[4]. Smith DS, Welch EB, Self-calibrated gradient delay correction for golden angle radial MRI, Proc ISMRM (2014) 1538.

[5]. Krämer M, Biermann J, Reichenbach JR, Intrinsic correction of system delays for radial magnetic resonance imaging, Magnetic Resonance Imaging 33 (2015) 491–496. doi:10.1016/j.mri.2015.01.005. [PubMed: 25601526]

[6]. Deshmane A, Blaimer M, Breuer F, Jakob P, Duerk J, Seiberlich N, Griswold M, Self-calibrated trajectory estimation and signal correction method for robust radial imaging using GRAPPA operator gridding, Magnetic Resonance in Medicine 75 (2016) 883–896. doi:10.1002/mrm.25648. [PubMed: 25765372]

[7]. Latta P, Starčuk Z, Gruwel ML, Weber MH, Tomanek B, K-space trajectory mapping and its application for ultrashort Echo time imaging, Magnetic Resonance Imaging 36 (2017) 68–76. doi:10.1016/j.mri.2016.10.012. [PubMed: 27742433]

[8]. Zhao X, Lee H, Song HK, Cheng CC, Wehrli FW, Impact of gradient imperfections on bone water quantification with UTE MRI, Magnetic Resonance in Medicine 84 (2020) 2034–2047. doi:10.1002/mrm.28272. [PubMed: 32307749]

[9]. Josan S, Pauly JM, Daniel BL, Pauly KB, Double half RF pulses for reduced sensitivity to eddy currents in UTE imaging., Magnetic Resonance in Medicine 61 (2009) 1083–9. doi:10.1002/mrm.21879. [PubMed: 19235919]

[10]. Josan S, Kaye E, Pauly JM, Daniel BL, Pauly KB, Improved half RF slice selectivity in the presence of eddy currents with out-of-slice saturation., Magnetic Resonance in Medicine 61 (2009) 1090–5. doi:10.1002/mrm.21914. [PubMed: 19319972]

[11]. Harkins KD, Does MD, Grissom WA, Iterative method for predistortion of MRI gradient waveforms., IEEE transactions on medical imaging 33 (2014) 1641–7. doi:10.1109/TMI.2014.2320987. [PubMed: 24801945]

[12]. Fabich HT, Benning M, Sederman AJ, Holland DJ, Ultrashort echo time (UTE) imaging using gradient pre-equalization and compressed sensing, Journal of Magnetic Resonance 245 (2014) 116–124. doi:10.1016/j.jmr.2014.06.015. [PubMed: 25036293]

[13]. Manhard MK, Harkins KD, Gochberg DF, Nyman JS, Does MD, 30-Second Bound and Pore Water Concentration Mapping of Cortical Bone Using 2D UTE With, Magnetic Resonance in Medicine 77 (2017) 945–950. doi:10.1002/mrm.26605. [PubMed: 28090655]

[14]. Grissom WA, Kerr AB, Stang PP, Lustig M, Scott GC, Pauly JM, GrIP : Gradient Iterative Predistortion for Multidimensional and Parallel Excitation, Proceedings of the 18th ISMRM 18 (2010) 4925.

[15]. Çavuşoğlu M, Mooiweer R, Pruessmann KP, Malik SJ, VERSE-guided parallel RF excitations using dynamic field correction, NMR in Biomedicine 30 (2017) 1–13. doi:10.1002/nbm.3697.

[16]. Abo Seada S, Price AN, Schneider T, Hajnal JV, Malik SJ, Multiband RF pulse design for realistic gradient performance, Magnetic Resonance in Medicine (2018) 1–15. doi:10.1002/mrm.27411.

[17]. Aigner CS, Rund A, Abo Seada S, Price AN, Hajnal JV, Malik SJ, Kunisch K, Stollberger R, Time optimal control-based RF pulse design under gradient imperfections, Magnetic Resonance in Medicine 83 (2020) 561–574. doi:10.1002/mrm.27955. [PubMed: 31441536]

[18]. Barmet C, De Zanche N, Pruessmann KP, Spatiotemporal magnetic field monitoring for MR, Magnetic Resonance in Medicine 60 (2008) 187–197. doi:10.1002/mrm.21603. [PubMed: 18581361]

[19]. De Zanche N, Barmet C, Nordmeyer-Massner J. a., Pruessmann KP, NMR probes for measuring magnetic fields and field dynamics in MR systems., Magnetic Resonance in Medicine 60 (2008) 176–86. doi:10.1002/mrm.21624. [PubMed: 18581363]

[20]. Onodera T, Matsui S, Sekihara K, Kohno H, A method of measuring field-gradient modulation shapes. Application to high-speed NMR spectroscopic imaging, Journal of Physics E: Scientific Instruments 20 (1987) 416–419. doi:10.1088/0022-3735/20/4/014.

[21]. Takahashi A, Peters T, Compensation of multi-dimensional selective excitation pulses using measuredk-space trajectories, Magnetic Resonance in Medicine 34 (1995) 446–456. doi:10.1002/mrm.1910340323. [PubMed: 7500885]

[22]. Papadakis NG, Wilkinson AA, Carpenter TA, Hall LD, A general method for measurement of the time integral of variant magnetic field gradients: Application to 2D spiral imaging, Magnetic Resonance Imaging 15 (1997) 567–578. doi:10.1016/S0730-725X(97)00014-3. [PubMed: 9254001]

[23]. Alley M, Glover G, Pelc N, Gradient characterization using a Fourier-transform technique, Magnetic Resonance in Medicine 39 (1998) 581–587. [PubMed: 9543420]

[24]. Malik SJ, Keihaninejad S, Hammers A, Hajnal JV, Tailored excitation in 3D with spiral nonselective (SPINS) RF pulses, Magnetic Resonance in Medicine 67 (2012) 1303–1315. doi:10.1002/mrm.23118. [PubMed: 21842503]

[25]. Duyn JH, Yang Y, Frank J. a., van der Veen JW, Simple correction method for k-space trajectory deviations in MRI., Journal of magnetic resonance (San Diego, Calif. : 1997) 132 (1998) 150–3. doi:10.1006/jmre.1998.1396.

[26]. Zhang Y, Hetherington HP, Stokely EM, Mason GF, Twieg DB, A novel k-space trajectory measurement technique., Magnetic Resonance in Medicine 39 (1998) 999–1004. [PubMed: 9621924]

[27]. Gurney P, Pauly J, Nishimura D, A Simple Method for Measuring B0 Eddy Currents, Proc. 13th Sci. Meeting, Int. Soc. … 132 (2005) 866.

[28]. Brodsky EK, Samsonov AA, Block WF, Characterizing and correcting gradient errors in non-Cartesian imaging: Are gradient errors Linear Time-Invariant (LTI)?, Magnetic Resonance in Medicine 62 (2009) 1466–1476. doi:10.1002/mrm.22100. arXiv:NIHMS150003. [PubMed: 19877274]

[29]. Gudbjartsson H, Patz S, The rician distribution of noisy mri data, Magnetic Resonance in Medicine 34 (1995) 910–914. doi:10.1002/mrm.1910340618. [PubMed: 8598820]

[30]. Addy NO, Wu HH, Nishimura DG, Simple method for MR gradient system characterization and k-space trajectory estimation., Magnetic Resonance in Medicine 68 (2012) 120–129. doi:10.1002/mrm.23217. [PubMed: 22189904]

[31]. Vannesjo SJ, Haeberlin M, Kasper L, Pavan M, Wilm BJ, Barmet C, Pruessmann KP, Gradient system characterization by impulse response measurements with a dynamic field camera., Magnetic Resonance in Medicine 69 (2013) 583–93. doi:10.1002/mrm.24263. [PubMed: 22499483]

[32]. Vannesjo SJ, Dietrich BE, Pavan M, Brunner DO, Wilm BJ, Barmet C, Pruessmann KP, Field camera measurements of gradient and shim impulse responses using frequency sweeps, Magnetic Resonance in Medicine 72 (2014) 570–583. doi:10.1002/mrm.24934. [PubMed: 24105800]

[33]. Goora FG, Colpitts BG, Balcom BJ, Arbitrary magnetic field gradient waveform correction using an impulse response based pre-equalization technique., Journal of Magnetic Resonance 238 (2014) 70–6. doi:10.1016/j.jmr.2013.11.003. [PubMed: 24316188]

[34]. Stich M, Wech T, Slawig A, Ringler R, Dewdney A, Greiser A, Ruyters G, Bley TA, Köstler H, Gradient waveform pre-emphasis based on the gradient system transfer function, Magnetic Resonance in Medicine 80 (2018) 1521–1532. doi:10.1002/mrm.27147. [PubMed: 29479736]

[35]. Rahmer J, Mazurkewitz P, Börnert P, Nielsen T, Rapid acquisition of the 3D MRI gradient impulse response function using a simple phantom measurement, Magnetic Resonance in Medicine (2019) mrm.27902. doi:10.1002/mrm.27902.

Highlights

- Variable-prephasing is proposed as a hybrid of previously published self-encoding and offset-slice gradient waveform measurement methods
- Variable-prephasing improves the precision of gradient waveform measurements by overcoming slice thickness limitations of the offset-slice method
- An algebraic model is introduced to optimally estimate gradient waveforms
- Experiments in phantoms were used to validate the theoretical predictions of the algebraic model

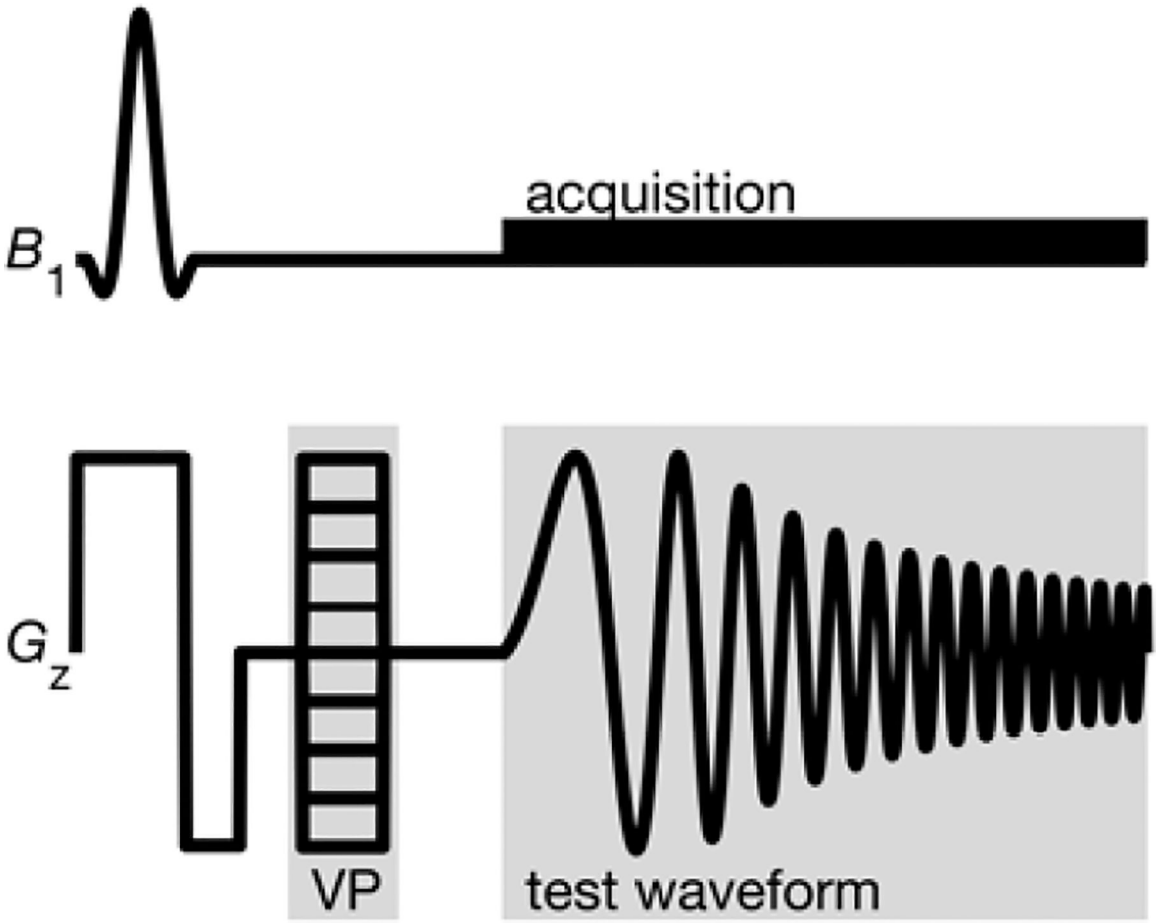

Figure 1:
The variable-prephasing pulse sequence uses a variable amplitude encoding gradient (v) in between slice excitation and test gradient waveform measurement.

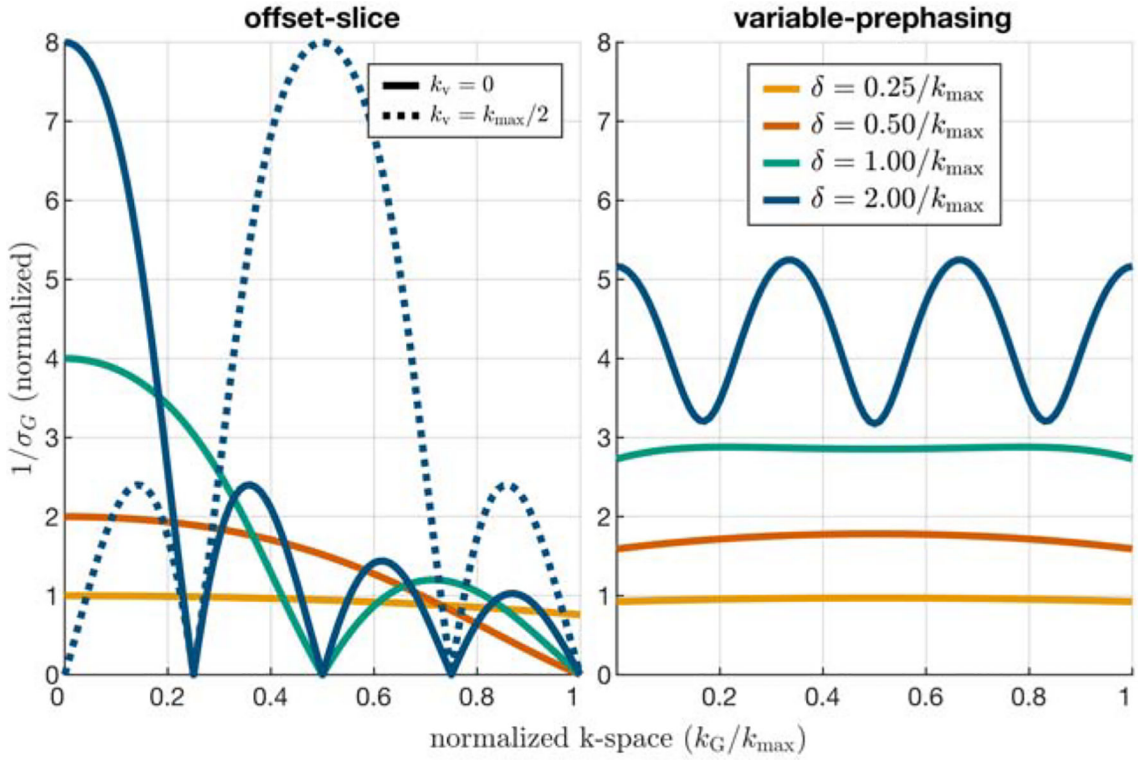

Figure 2:

Gradient waveform measurement precision per excitation. In offset slice gradient waveform methods (left), precision is limited by the maximum area of the test gradient waveform. Thin slices can be used to produce low but uniform precision, while precision in larger slices can vary widely. By changing the area of the VP gradient, the envelope of the signal can be shifted (shown as the dashed line, for $k_v = -k_{max}/2$). The precision of the gradient waveform measurement (shown with $N_v = N_0 = 4$) can be improved over the whole domain of k_G by combining multiple measurements over a range of VP gradient areas (shown right).

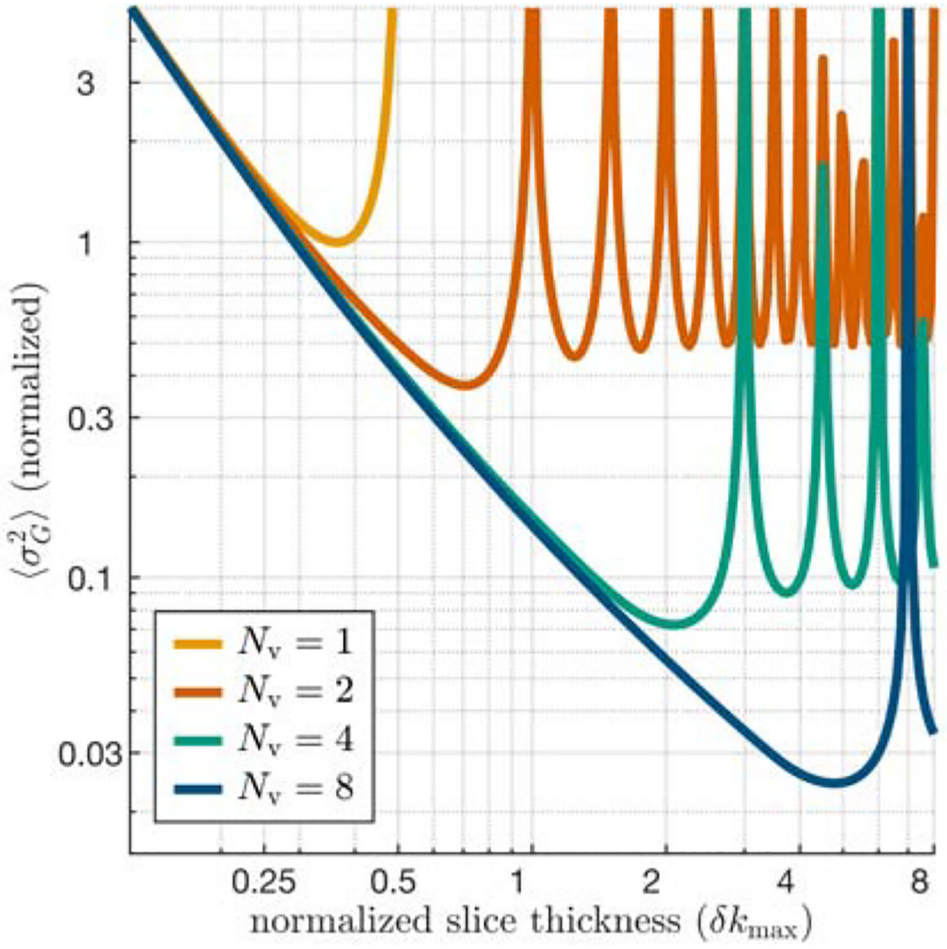

Figure 3:

By increasing the number of VP steps (N_v), thicker slices reduce the average variance of the gradient waveform measurement. For large N_v, $\langle \sigma_G^2 \rangle$ is minimized at approximately $\delta k_{max} N_v/2$. For all curves, $N_0 = N_v$.

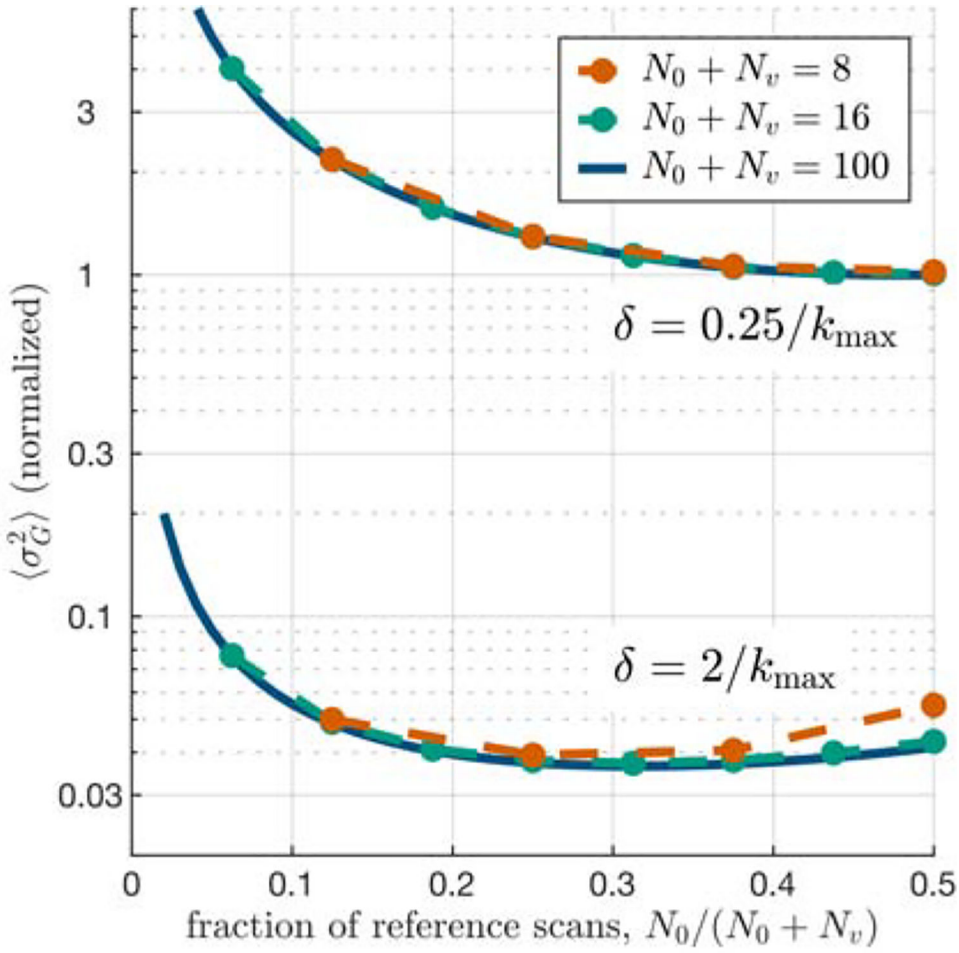

Figure 4:

Trading in variance between N_0 reference scans with N_v acquisitions. With the total number of acquisitions given by $N_0 + N_v$, the fraction of total scan time that optimizes the variance depends upon slice thickness, varying between 30%−50% of the total acquisition time.

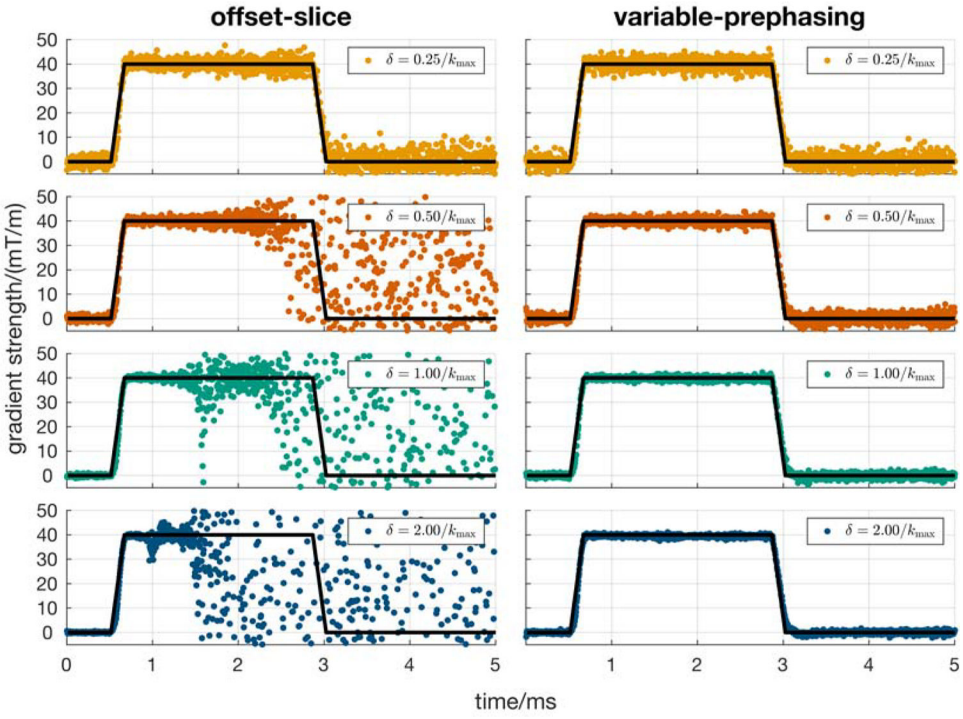

Figure 5:

Measured trapezoidal gradient waveforms. For the thin slices ($\delta_z = 0.25/k_{max}$), the offset slice and VP gradient waveform measurement methods both provide low precision estimates of the applied gradient waveform. While the precision of the offset-slice method suffers with increased slice thickness, VP can be used to improve precision of the gradient waveform measurement.

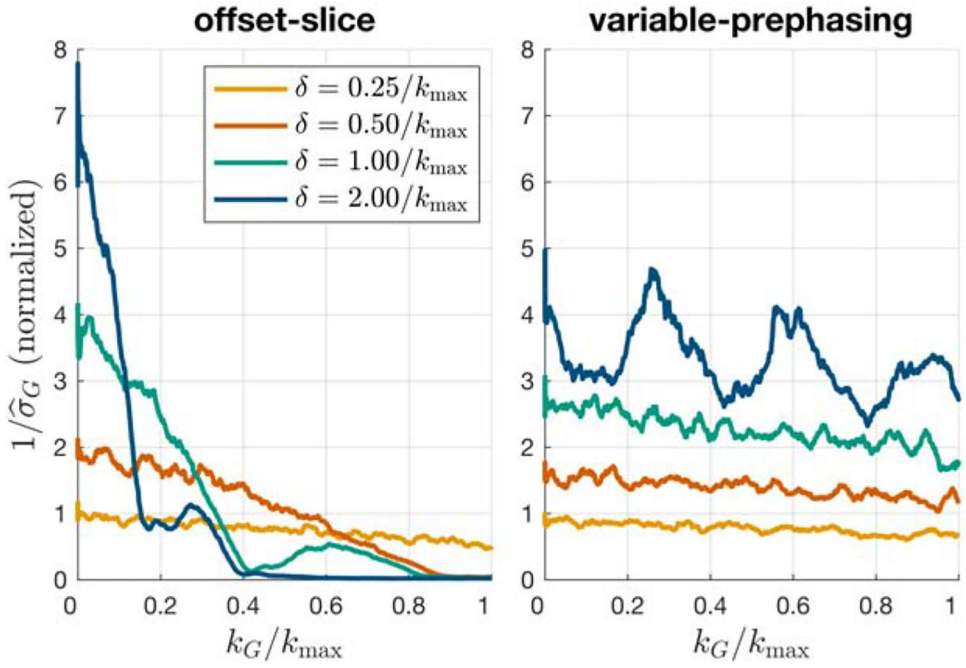

Figure 6:

Measured precision per excitation. The precision of the test gradient waveform measurement was estimated from 16 repetitions, and closely matches theoretical predictions plotted in Figure 2.